Pairing core swelling effect in Pb isotopes at $N > 126$

W. Horiuchi [1,*] and T. Inakura [2]

[1] *Department of Physics, Hokkaido University, Sapporo 060-0810, Japan*

[2] *Laboratory for Zero-Carbon Energy, Institute of Innovative Research, Tokyo Institute of Technology, Tokyo 152-8550, Japan*

(Received 12 January 2022; accepted 24 March 2022; published 7 April 2022)

We revisit a sudden increase of the isotope shift of the charge radius of Pb isotopes at $N > 126$ based on a Skyrme Hartree-Fock-Bogoliubov theory. New parametrizations of the pairing interaction optimized for four selected Skyrme interactions greatly improve a description of this phenomenon. The density-dependent spin-orbit interaction is also investigated and further increases the charge radius. The pairing correlations significantly change the properties of the neutron orbits near the Fermi level and play a vital role in pulling out the well-bound protons in the Pb isotopes at $N > 126$. Regarding ^{208}Pb as a "core" nucleus, a novel pairing core swelling effect is proposed: The pairing interaction reduces the radius of "valence" neutron orbits by the shrinkage of the diffused $1g_{9/2}$ orbit and the mixing of the sharp $0i_{11/2}$ orbit. Simultaneously, the core nucleus swells, leading to the sudden enhancement of the charge radius at $N > 126$. This characteristic behavior appears in the density profile near the nuclear surface and its measurement is highly desirable.

DOI: 10.1103/PhysRevC.105.044303

I. INTRODUCTION

The nuclear radii are fundamental quantities that reflect characteristics of the density profile of atomic nuclei. Systematic measurements of nuclear charge radii have been done by using electron scattering for stable nuclei and have been extended for short-lived unstable nuclei with isotope-shift measurements. It is known that the mass number A dependence of the charge radius is roughly proportional to $A^{1/3}$. For spherical nuclei, this slope changes across the magic numbers, where the major shell changes [1]. Recently, a sudden increase or a kink of the charge radius at $N > 28$ was found in the charge radius measurement of Ca isotopes [2] and has attracted much attention. The phenomenon was interpreted as the swelling of a ^{48}Ca "core" in the interaction cross section measurement [3]. Later, this mechanism was related to the saturation of the internal density [4]. However, a universal understanding has not been reached for all mass regions including heavier mass nuclei such as Pb isotopes.

The charge radius kink observed in Pb isotopes at $N > 126$ is one of the most famous examples. To describe the properties of such heavy mass nuclei, a Skyrme-type density functional [5] has often been used. Reference [6] pointed out that a conventional Skyrme Hartree-Fock calculation cannot reproduce the kink behavior and introduced the isospin-dependent spin-orbit interaction. Reference [7] introduced the density-dependent spin-orbit (DDLS) interaction and showed that the kink behavior was better explained by considering both the configuration mixing and modification of the $1g_{9/2}$ and $0i_{11/2}$ orbits. We remark that the Fayans effective interaction reproduced the kink behavior of the charge radii [8] but the relation of those kinks to the interaction was not clear. Recently, the charge radius kink at $N > 126$ was observed also in Hg isotopes [9,10] showing that the charge radius kink is a universal phenomenon whose emergence mechanism should be clarified.

In this paper, we revisit the kink behavior of Pb isotopes at $N > 126$ based on a Hartree-Fock-Bogoliubov (HFB) theory with a Skyrme density functional. To describe the charge radius kink of heavy mass regions, it is vital to properly treat the pairing and spin-orbit interactions [6,7]. The purpose of this paper is twofold: (i) We give appropriate parametrizations for the pairing and DDLS interactions optimized for several standard Skyrme interactions, and then (ii) analyze size properties of the Pb isotopes and clarify the role of the pairing correlations and DDLS interaction in producing the charge radius kink.

The paper is organized as follows. Section II briefly describes the HFB theory with the Skyrme density functional. The pairing and DDLS interactions include some free parameters. Section III explains how to fix them by using experimental data. Section IV presents our results. Results of the isotope shift of the charge radius are compared with experimental data in Sec. IV A. The importance of the pairing correlations is emphasized to reproduce the charge radius kink of the Pb isotopes. The DDLS further enhances the charge radius though it is not more significant than the pairing correlations. The kink at $N > 126$ is induced by the pairing interaction and is interpreted as a swelling of the "core." Section IV B describes the mechanism of this pairing core swelling phenomenon in detail. The influence on observables other than the charge radius is discussed in Sec. IV C for future measurements. The conclusion is given in Sec. V.

*whoriuchi@nucl.sci.hokudai.ac.jp

II. THEORETICAL MODELS

The density functional theory (DFT) is one of the standard approaches to investigate nuclear properties in a systematic way. The DFT with the Skyrme functional describes the ground-state energy as a functional of three one-body densities, i.e., nucleon $\rho_q(\boldsymbol{r})$, kinetic $\tau_q(\boldsymbol{r})$, and spin-orbit $\boldsymbol{J}_q(\boldsymbol{r})$ densities, where q denotes neutron (n) or proton (p). In the HFB formalism with spherical symmetry, the Hamiltonian is reduced to the mean field h (particle-hole channel) and the pairing field Δ (particle-particle channel) as

$$\begin{pmatrix} (h-\lambda) & \Delta \\ -\Delta^* & -(h-\lambda)^* \end{pmatrix} \begin{pmatrix} U_k(r) \\ V_k(r) \end{pmatrix} = E_k \begin{pmatrix} U_k(r) \\ V_k(r) \end{pmatrix}, \quad (1)$$

where U_k and V_k are the two components of the single-quasiparticle radial wave functions and E_k is their energy, and λ is the chemical potential. We use $k = nlj$ as a shorthand notation for the quantum numbers of the system, where n, l, and j are the number of nodes, orbital angular momentum, and total angular momentum, respectively.

Calculations are performed for Pb isotopes by using the HFB solver HFBRAD [11], which solves the Skyrme HFB equations in the coordinate representation with spherical symmetry. The model space is set to the radius $R_{\rm box} = 25$ fm with mesh spacing 0.1 fm. The maximum values for the angular momentum of the quasiparticle orbits are set to be $j_{\rm max} = (55/2)\hbar$ for neutrons and $(45/2)\hbar$ for protons. We choose four standard Skyrme functionals in the particle-hole channels: SkM* [12], SLy4 [13], SV-min [14], and UNEDF1 [15]. The SkM* and SLy4 interactions have been widely used for nuclear structure calculations, and SV-min and UNEDF1 were recently designed as sophisticated versions of Skyrme parameter sets. For the particle-particle channel, we employ the mixed-type pairing

$$V_{\rm pair}(\boldsymbol{r}, \boldsymbol{r}') = V_0 \left(1 - \frac{1}{2}\frac{\rho(\boldsymbol{r})}{\rho_0}\right) \delta(\boldsymbol{r} - \boldsymbol{r}'), \quad (2)$$

where $\rho_0 = 0.16$ fm^{-3} and V_0 is the pairing strength that will be adjusted later. All the single-quasiparticle states below a cutoff energy $E_{\rm cut} = 60$ MeV are considered for all the interactions, while a state-dependent energy cut-off was conventionally used for SV-min [14]. Therefore, our results labeled with SV-min are somewhat different from those with the original SV-min interaction.

References [7,16] suggest the need for the density-dependent spin-orbit (DDLS) interaction to explain the kink behavior in the isotope shift of the charge radius of Pb isotopes. Here we consider adapting it to the Skyrme functionals. The spin-orbit energy functional of the Skyrme interaction is explicitly written as [5]

$$E_{\rm LS} = -\int d\boldsymbol{r}\, W_{\rm LS} \times \left\{ \rho \nabla \cdot \boldsymbol{J} + \sum_q \rho_q \nabla \cdot \boldsymbol{J}_q - \boldsymbol{J} \cdot \nabla \rho - \sum_q \boldsymbol{J}_q \cdot \nabla \rho_q \right\}, \quad (3)$$

where $\rho = \rho_n + \rho_p$ and $\boldsymbol{J} = \boldsymbol{J}_n + \boldsymbol{J}_p$ with

$$W_{\rm LS} = \tfrac{1}{4} W_0. \quad (4)$$

This $W_{\rm LS}$ term is simply replaced by [7,16]

$$W_{\rm DDLS} = f_{ls} \frac{W_0}{4} + g_{ls} D[\rho(\boldsymbol{r})], \quad (5)$$

where f_{ls} and g_{ls} are free parameters to be determined later. A functional form of the density-dependent term $D[\rho(\boldsymbol{r})]$ is taken as

$$D[\rho(\boldsymbol{r})] = w_1 \frac{\rho(\boldsymbol{r})}{1 + d_1 \rho(\boldsymbol{r})} \quad (6)$$

with $w_1, d_1 > 0$. The second term in the denominator sets the upper limit of D as $|D| < w_1/d_1$ at extremely high density regions. We adopt $d_1 = 1.0$ fm^3 and $w_1 = 742$ MeV fm^8 as prescribed in Ref. [7].

Once the HFB equation is solved, we can evaluate various observables. The single-quasiparticle orbit includes the fractional occupation of the single-particle (sp) orbit, indicating the mixing of the sp orbits. It is useful to evaluate the occupation probability n_k and sp radius r_k for the k orbital as

$$n_k = 4\pi \int_0^\infty dr\, r^2 |V_k(r)|^2, \quad (7)$$

$$r_k = \sqrt{\frac{4\pi}{n_k} \int_0^\infty dr\, r^4 |V_k(r)|^2}. \quad (8)$$

The second-order moment of the nuclear charge distribution is given by [17]

$$r_{\rm ch}^2 = \langle r^2 \rangle_p + r_p^2 + (r_+^2 - r_-^2)\frac{N}{Z} + \langle r^2 \rangle_{W_p} + \langle r^2 \rangle_{W_n} \frac{N}{Z} + \delta \langle r^2 \rangle_c, \quad (9)$$

where $r_p = 0.81$ fm, $r_\pm^2 = (0.9)^2 \mp 0.06$ fm^2. The point neutron/proton density and spin-orbit density are given by

$$\langle r^2 \rangle_q = \frac{4\pi}{N_q} \int_0^\infty dr\, r^4 \rho_q(r), \quad (10)$$

$$\langle r^2 \rangle_{W_q} = -\frac{\mu_q (\hbar c)^2}{2(Mc^2)^2} \frac{4\pi}{N_q} \int_0^\infty dr\, r^4 \nabla \cdot \boldsymbol{J}_q(r), \quad (11)$$

where $q = n$ or p, namely, $N_n = N$, $N_p = Z$, $\mu_n = 1.793$, $\mu_p = -1.913$, and M is the nucleon mass. The last term is the relativistic correction:

$$\delta \langle r^2 \rangle_c = \frac{3(\hbar c)^2}{4(Mc^2)^2} + \frac{1}{2\mu_p} \langle r^2 \rangle_{W_p}. \quad (12)$$

III. ADJUSTMENT OF PARAMETERS

The pairing interaction plays a vital role to determine the configuration mixing near the Fermi level. The pairing strength has been conventionally determined in such a way that theoretically obtained pairing gaps in even-even nuclei reproduce experimental odd-even mass differences. However, no direct relationship between the calculated pairing gap and the experimental odd-even mass exists, and there are a variety

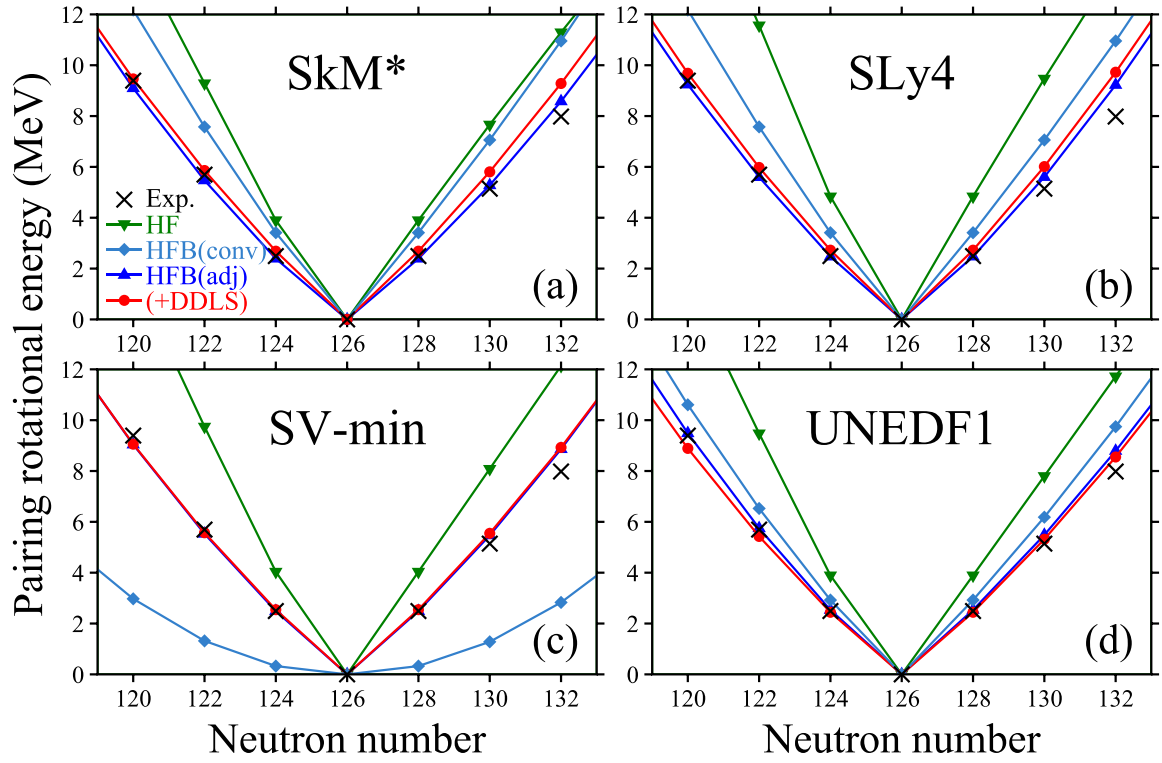

FIG. 1. Neutron pairing-rotational energies measured from a reference state, ^{208}Pb, for (a) SkM*, (b) SLy4, (c) SV-min, and (d) UNEDF1 interactions. HFB(conv) and HFB(adj) respectively indicate the HFB calculations with the conventional and present parametrizations of the pairing strength. See text for details. Experimental (black) values are evaluated from the experimental binding energies taken from Ref. [25] by using Eq. (13).

of definitions of theoretical pairing gaps and ways of extracting the odd-even mass difference from experiment [18–20]. Recently, Ref. [21] proposed a new sound procedure to determine the pairing strength using the pairing-rotational energy. The pairing-rotational energy is defined by the second-order term of the ground-state energy expanded in the neutron number $\Delta N = N - N_0$ as

$$E(N, Z_0) = E(N_0, Z_0) - \lambda_n(N_0, Z_0)\Delta N + \frac{(\Delta N)^2}{2\mathfrak{I}(N_0, Z_0)}, \tag{13}$$

where $E(N_0, Z_0)$ denotes the ground-state energy of a nucleus with neutron number N_0 and proton number Z_0, $\lambda_n(N_0, Z_0) = dE/dN|_{N=N_0} \equiv [E(N_0 - 2, Z_0) - E(N_0 + 2, Z_0)]/4$ is the chemical potential. The last term of Eq. (13) is the pairing-rotational energy, which can be evaluated only by using the experimental data for even-even nuclei. In the present study, the pairing strength V_0 of Eq. (2) is determined so as to reproduce the pairing-rotational energy around ^{208}Pb ($N_0 = 126$ and $Z_0 = 82$) for each Skyrme functional.

Next, we explain how to implement the DDLS interaction in the Skyrme functionals [see Eq. (5)]. We will seek values of the two parameters f_{ls} and g_{ls} to reproduce the isotope shift of the charge radius of Pb isotopes at $N > 126$. In this procedure, we pay special attention to the neutron sp level ordering around the Fermi level in ^{208}Pb. It is known that neutron sp levels around the Fermi level ($2p_{1/2}$) are $0i_{13/2}$, $2p_{3/2}$, $1f_{5/2}$, $2p_{1/2}$, $1g_{9/2}$, $0i_{11/2}$, and $0j_{15/2}$ in order [22–24]. As was pointed out in Ref. [7], if the $0i_{11/2}$ orbit is located below the $1g_{9/2}$ orbit, the charge radius increases at $N > 126$ drastically. However, it contradicts the ordering of the sp levels, which should be preserved. Thus, we implement the DDLS and tune the parameters f_{ls} and g_{ls} under the condition that the neutron sp level ordering is consistent with experimental data. We do not pay much attention to the ordering of three higher nodal orbitals $2p_{3/2}$, $1f_{5/2}$, and $2p_{1/2}$ as they are almost degenerate and have a small impact on changes in the isotope shift. After we find optimal f_{ls} and g_{ls} values, we reoptimize the pairing strengths V_0 by following the procedure explained in the previous paragraph. Hereafter we examine the following three types of calculations: HF (without the pairing and DDLS interactions), HFB (with the pairing interaction and without the DDLS interaction), and HFB + DDLS (with the pairing and DDLS interactions).

Figure 1 displays the pairing-rotational energies measured from a reference state, ^{208}Pb, as a function of the neutron number for the SkM*, SLy4, SV-min, and UNEDF1 functionals. We see that without the pairing correlations the HF calculations do not reproduce the pairing-rotational energy around ^{208}Pb deduced from the experimental data. With the optimized pairing and DDLS parameters, the HFB(adj) and HFB + DDLS calculations nicely reproduce the experimental data for all the Skyrme interactions employed in this paper. To show further improvement with this parameter set, Fig. 2 plots two-neutron separation energies obtained by HF, HFB, and

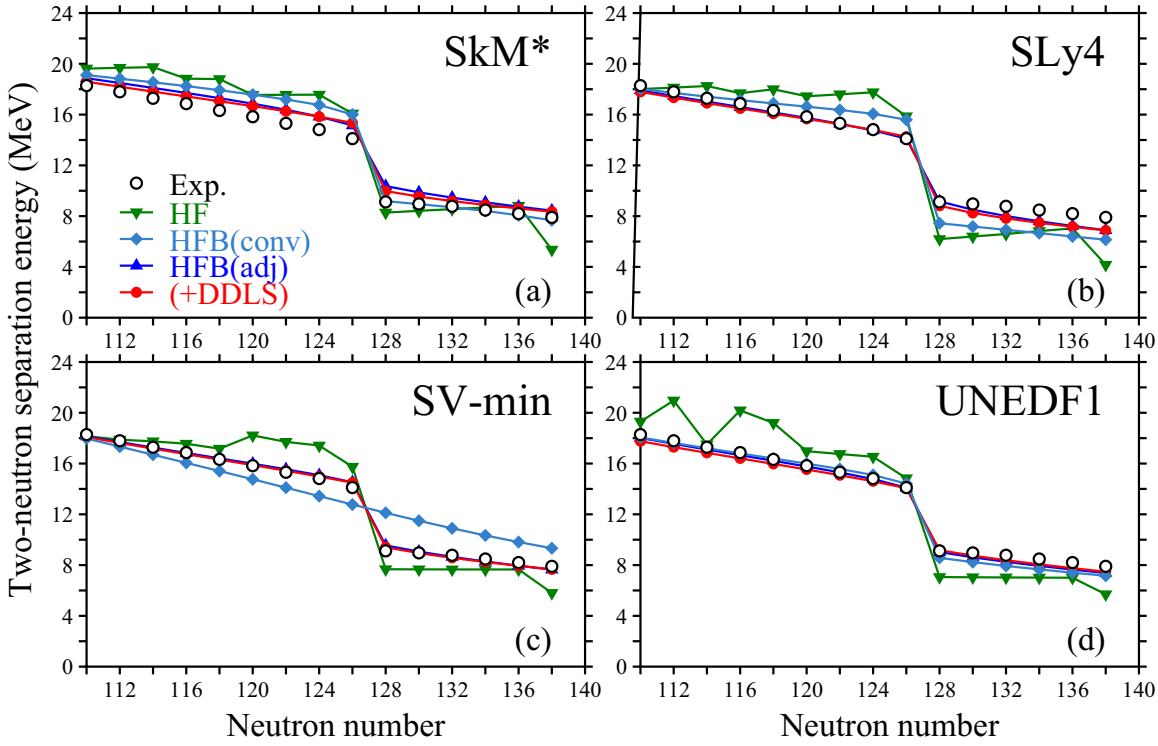

FIG. 2. Two-neutron separation energies of Pb isotopes for (a) SkM*, (b) SLy4, (c) SV-min, and (d) UNEDF1 interactions. Experimental data are taken from [25]. HFB(conv) and HFB(adj) respectively indicate the HFB calculations with the conventional and present parametrizations of the pairing strength. See text for details.

HFB + DDLS calculations. The HFB(adj) and HFB + DDLS results are greatly improved compared to the results of HF and correctly describe the experimental data.

For the sake of comparison, we also show the results with the conventional parametrization for the pairing interaction, in which a fixed pairing strength is used for nuclei covering the whole nuclear chart [HFB(conv)]. For SkM* and SLy4, the pairing strengths are tuned to give a mean neutron gap of 1.245 MeV in ^{120}Sn [11]. The pairing strength of UNEDF1 is determined together with other Skyrme parameters to reproduce nuclear matter properties and nuclear masses [15]. For SV-min, odd-even staggering is employed to determine the pairing strength [14]. We see that the reproducibility of the experimental pairing rotational energy and two-neutron separation energies is not good with the conventional pairing strengths. Describing the pairing rotational energies is important to determine the pairing strength. For the convenience of the reader, we list all the optimized values of the pairing strength V_0, f_{ls}, and g_{ls} in the DDLS interaction in Table I. The following discussions will be made based on the results obtained with these parameter sets.

IV. RESULTS AND DISCUSSION

A. Charge radius kink and pairing correlations

Figure 3 plots the difference of the squared charge radii of Pb isotopes $r^2_{\rm ch}(N)$ from that of ^{208}Pb, defined by

$$\Delta r^2_{\rm ch} = r^2_{\rm ch}(N) - r^2_{\rm ch}(N_0) \tag{14}$$

with $N_0 = 126$. Neither HF calculation adopted here reproduces the kink structure at $N = 126$, while a clear kink appears at $N = 126$ when the proper pairing correlations are included [HFB(adj)]. We also plot the results with the conventional parametrization for the pairing interaction [HFB(conv)], showing less reproducibility of the experimental data as was already pointed out in Ref. [27]. Hereafter we only discuss the results with the present parametrization [HFB(adj)] as the HFB calculation. In the present choice of the pairing strength, the HFB calculation already describes the kink behavior and is slightly improved by the HFB + DDLS calculation for all the Skyrme-type interactions adopted in this paper. The agreement between the theory and experiment is satisfactory: as good as that obtained in Ref. [7]. We remark that in Ref. [7] the DDLS effect appeared to be more drastic than the present results because of the different choices of the pairing and energy functionals.

TABLE I. Pairing strength V_0 and the parameters of the DDLS interaction, f_{ls} and g_{ls}, adopted in the present work.

	HFB			HFB+DDLS		
	V_0 (MeV)	f_{ls}	g_{ls}	V_0 (MeV)	f_{ls}	g_{ls}
SkM*	−269	1.00	0.00	−269	0.75	0.15
SLy4	−321	1.00	0.00	−323	0.80	0.20
SV-min	−243	1.00	0.00	−246	0.80	0.20
UNEDF1	−248	1.00	0.00	−246	0.80	0.10

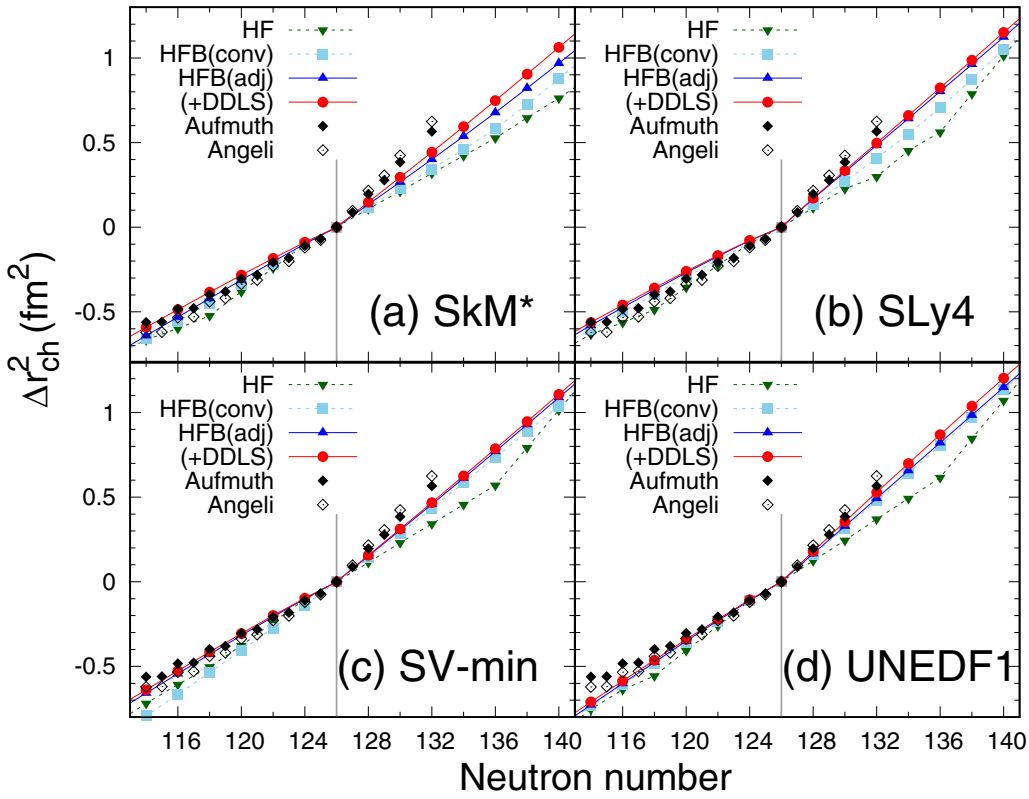

FIG. 3. Absolute difference of squared charge radii of Pb isotopes from that of ^{208}Pb as a function of the neutron number with HF, HFB, and HFB + DDLS calculations. HFB(conv) and HFB(adj) respectively indicate the HFB calculations with the conventional and present parametrizations of the pairing strength. See text for details. The vertical lines indicate $N = 126$. The (a) SkM*, (b) SLy4, (c) SV-min, and (d) UNEDF1 interactions are employed. Experimental data are taken from Refs. [1,26].

B. Pairing core swelling effect at $N > 126$

We see that the large enhancement of the charge radius in Pb isotopes for $N > 126$ is well reproduced by the inclusion of the adjusted pairing interaction. This kink behavior is an indication of "core" swelling, which was recently discussed for Ca isotopes for $N > 28$ in the charge radius measurement [2] and interaction cross section measurement [3]. Here we show that this sudden core swelling for Pb isotopes can also be understood by considering the mechanism recently proposed in Ref. [4] for spherical nuclei: The occupation of nodal or j-lower ($j_< = l - 1/2$ with $l > 0$) orbits can induce a sudden swelling of the "core" because the density distributions of those orbits have a large overlap with the internal or core density [4]. We remark that the configuration mixing regarding nuclear deformation was discussed in Ref. [28]. In the present paper, we define the core nucleus as ^{208}Pb for $N > 126$ and discuss the role of the valence neutrons in this core swelling phenomenon. We note that for $N > 126$ the quantum number of the lowest orbit is $1g_{9/2}$. However, as we see in Fig. 3, the charge radius kink or the core swelling is not enough in the HF calculation even though the nodal $1g_{9/2}$ orbit is filling for $N = 126-136$.

To understand the role of the pairing and DDLS interactions in the core swelling phenomena in detail, we list in Table II the occupation numbers of the $1g_{9/2}$, $0i_{11/2}$, and $0j_{15/2}$ orbits and various root-mean-square (rms) radii of ^{214}Pb obtained by the HF, HFB, and HFB + DDLS calculations. In the HF calculation, all the "valence" neutrons occupy the lowest $1g_{9/2}$ level as $n(1g_{9/2}) = 6$. By including the pairing correlations, the occupation number is shared with the three orbits $1g_{9/2}$, $0i_{11/2}$, and $0j_{15/2}$. The sum of their occupation numbers, $n_v = n(1g_{9/2}) + n(0i_{11/2}) + n(0j_{15/2})$, is close to 6. Therefore, these three orbits can be regarded as the "valence" neutron orbits for ^{214}Pb.

Here, we see that the pairing correlations significantly change the rms sp radii of the $1g_{9/2}$ orbit and induce the mixing of the $1g_{9/2}$, $0i_{11/2}$, and $0j_{15/2}$ orbits. References [6,7] pointed out that the mixing of the $0h_{11/2}$ orbit is a key to the understanding of the kink behavior at $N > 126$. Without the pairing correlations, the $1g_{9/2}$ orbits still have a large rms sp radius. The pairing correlations play a role to reduce the size of the $1g_{9/2}$ orbit and induce the mixing of the $0i_{11/2}$ orbit. We note that the $0i_{11/2}$ orbit has a smaller rms radius than the $1g_{9/2}$ orbit. Both the effects facilitate the core swelling because an overlap between the valence and core densities becomes large by the same mechanism proposed in Ref. [4]. The pairing correlations also induce the mixing of the $0j_{15/2}$ orbit but its contribution to the core swelling is expected to be not large. Because the orbit is nodeless and j-upper, and its rms sp radius is the largest among the three main orbits of the valence neutrons, the probability of finding these neutrons is distributed mostly near the nuclear surface.

TABLE II. Occupation numbers and rms sp neutron radii, in units of fm, of ^{214}Pb near the Fermi level and those for the valence neutrons (n_v and r_v). See text for details. Charge ($r_{\rm ch}$), rms point-proton (r_p), neutron (r_n), and matter (r_m) radii are also listed in units of fm.

	SkM*			SLy4			SV-min			UNEDF1		
	HF	HFB	(+DDLS)	HF	HFB	(+DDLS)	HF	HFB	(+DDLS)	HF	HFB	(+DDLS)
$n(1gf_{9/2})$	6	3.68	3.47	6	3.13	3.02	6	3.29	3.46	6	3.09	2.70
$n(0i_{11/2})$		0.76	1.30		1.56	1.78		1.50	1.41		1.51	2.16
$n(0j_{15/2})$		1.40	0.97		1.10	0.94		0.91	0.83		1.15	0.88
n_v	6	5.84	5.74	6	5.80	5.74		5.71	5.74	6	5.76	5.74
$r(1g_{9/2})$	6.57	6.47	6.48	6.71	6.56	6.57	6.49	6.37	6.38	6.53	6.41	6.40
$r(0i_{11/2})$		6.31	6.36		6.39	6.41		6.27	6.29		6.25	6.28
$r(0j_{15/2})$		6.68	6.68		6.74	6.73		6.58	6.61		6.61	6.61
r_v	6.57	6.50	6.49	6.71	6.55	6.55	6.49	6.38	6.39	6.53	6.41	6.39
$r_{\rm ch}$	5.52	5.54	5.55	5.53	5.55	5.55	5.52	5.53	5.53	5.54	5.55	5.56
r_p	5.48	5.49	5.50	5.49	5.50	5.50	5.48	5.49	5.48	5.49	5.50	5.51
r_n	5.69	5.69	5.70	5.69	5.70	5.70	5.69	5.69	5.68	5.70	5.70	5.71
r_m	5.61	5.62	5.63	5.61	5.62	5.62	5.61	5.61	5.60	5.62	5.63	5.63

We discuss the role of the DDLS interaction. As expected from the results in Ref. [7], the DDLS plays a role to increase (decrease) the radii of $j_<$ ($j_> = l + 1/2$) orbits. In fact, the rms sp radius of the $0i_{11/2}$ is enhanced by the DDLS interaction. At the same time, the DDLS interaction also induces a little change of the configuration mixing of the $1g_{9/2}$, $0i_{11/2}$, and $0j_{15/2}$ orbits. In the present cases, the DDLS mainly enhances the rms sp radius of the $0i_{11/2}$ orbit; e.g., for SkM*, the enhancement is about 0.05 fm from that of the HFB result, while the radius of the $0i_{13/2}$ orbit is almost unchanged by 0.005 fm as the orbit belongs to the "core." Consequently, its radius becomes closer to that of the $0i_{13/2}$, 6.42 fm, resulting in a larger overlap between the core and valence nucleon densities and hence the core swells.

We also calculate the average rms sp radius of the valence neutrons defined by

$$r_v^2 = \frac{\sum_{\bar{n},\bar{l},\bar{j}\in v} n(\bar{n}\bar{l}_{\bar{j}}) r^2(\bar{n}\bar{l}_{\bar{j}})}{\sum_{\bar{n},\bar{l},\bar{j}\in v} n(\bar{n}\bar{l}_{\bar{j}})}. \tag{15}$$

Here $\bar{n}\bar{l}\bar{j}$ runs over $1g_{9/2}$, $0i_{11/2}$, and $0j_{15/2}$. The results are listed in Table II. Note that the r_v value of the HF calculation corresponds to the rms sp radius of $1g_{9/2}$ orbit. The pairing interaction reduces the radius of $1g_{9/2}$ and increases the mixing probability of the $0i_{11/2}$, which has a smaller sp radius compared to the others. The $0j_{15/2}$ orbit has the largest radius among the others but the occupation number is small. In total, the rms radius of the valence neutrons is significantly reduced by the pairing interaction. An interesting observation is that the proton and neutron rms radii are enhanced when the pairing correlations are included despite the rms radius of the valence neutrons being reduced. The pairing correlation induces the core swelling. We remark that Ref. [29] argued that the pairing correlation reduces the charge radius kink at $N > 126$ based on the covariant density functional theory. Because in the covariant density functional theory the $0i_{11/2}$ energy is lower than the $1g_{9/2}$ one, the occupation number of the $0i_{11/2}$ orbit is reduced when the pairing interaction is included, which is in contrast to the present Skyrme density functional cases. We find that the DDLS interaction plays a role in reducing the rms radius of the valence neutrons for all the Skyrme interactions and further enhances the rms proton radius. The reduction of the valence neutron radius is essential to induce the core swelling.

Figure 4 plots the occupation numbers of the $1g_{9/2}$, $0i_{11/2}$, and $0j_{15/2}$ orbits, which give the three largest occupations for the Pb isotopes at $N > 126$, as a function of the neutron number. We also show the occupation numbers of the sum of these three orbits. Since these sums almost follow $N - 126$ with $126 < N < 140$, these three orbits can still be regarded as the valence neutrons as the contributions from higher-lying orbits, i.e., the $1g_{7/2}$, $2d_{5/2}$, $3s_{1/2}$, and $2d_{3/2}$ orbits, are still not large in this mass region, at most $\approx 1/14$ of the valence neutrons at $N = 140$. By including the DDLS interaction, as expected from Ref. [7], a relatively large enhancement of the occupation of $0i_{11/2}$ orbit is obtained for SkM* and UNEDF1, while the occupation number of the $0j_{15/2}$ orbit is reduced. Since all the orbits other than the $0j_{15/2}$ orbit can contribute to swelling the core [4], further core swelling is expected when the DDLS interaction is implemented. In fact, the rms valence neutron orbits reduces and the rms proton radius is enhanced by the inclusion of the DDLS interaction. We note that in Fig. 3 the improvement of the charge radius results was not significant for the SLy4 and SV-min interactions. Because the pairing correlations already incorporate possible reduction of the valence neutron orbits, there is no room to enhance the proton radius with the inclusion of the DDLS interaction. In fact, virtually no change is obtained in the occupation numbers with the HFB and HFB + DDLS results for SLy4 and SV-min, as seen in Fig. 4.

For larger N regions for $N > 140$, in addition to the three main orbits the occupation numbers of the $1g_{7/2}$, $2d_{5/2}$, $3s_{1/2}$, and $2d_{3/2}$ orbits become large. They are nodal orbits that can have a large overlap with the sp density in the internal regions. Further development of the core swelling is expected for $N > 140$.

C. Effects of the pairing correlations to other observables

It is also interesting to note that the matter radius increases even though the valence neutron orbits shrink by the

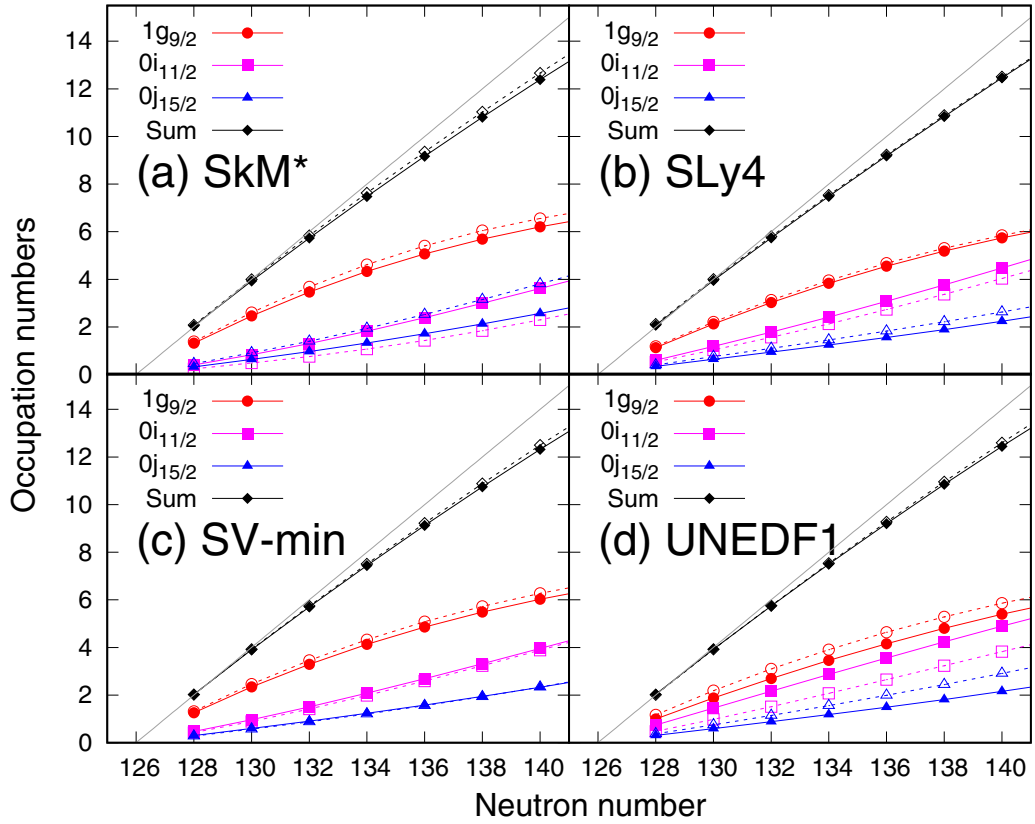

FIG. 4. Occupation numbers of the $1g_{9/2}$, $0i_{11/2}$, and $0j_{15/2}$ orbits of Pb isotopes calculated with HFB (open symbols with dashed lines) and HFB + DDLS (closed symbols with solid lines). The sums of these occupation numbers are also drawn. The line indicates the $N - 126$ line, which corresponds to the maximum occupation numbers in the assumption of $N = 126$ closed configuration for the ^{208}Pb core. The (a) SkM*, (b) SLy4, (c) SV-min, and (d) UNEDF1 interactions are employed.

pairing interaction. In this last subsection, we discuss how this structure change affects the density profile or the nuclear size properties. Figure 5 plots the neutron skin thickness, defined by $\Delta r_{np} = r_n - r_p$, of Pb isotopes at $114 < N < 140$. In the HF calculation [Fig. 5(a)], some wiggles are found due to changes of the outermost neutron orbits, e.g., from $1g_{9/2}$ to $0i_{11/2}$ at $N = 136$. In the HFB and HFB + DDLS calculations respectively drawn in Figs. 5(b) and 5(c), we do not see that ill behavior, showing that the neutron skin thickness is a robust quantity. The neutron number dependence of the skin thickness exhibits good linearity with small interaction dependence, if the pairing interaction is properly chosen.

The HFB and HFB + DDLS calculations induce the mixing of the main three orbits $1g_{9/2}$, $0i_{11/2}$, and $0j_{15/2}$ for $N > 126$. The occupation probabilities of the sp orbits near the Fermi level strongly affect the density distribution near the nuclear surface. Determining such density profiles is

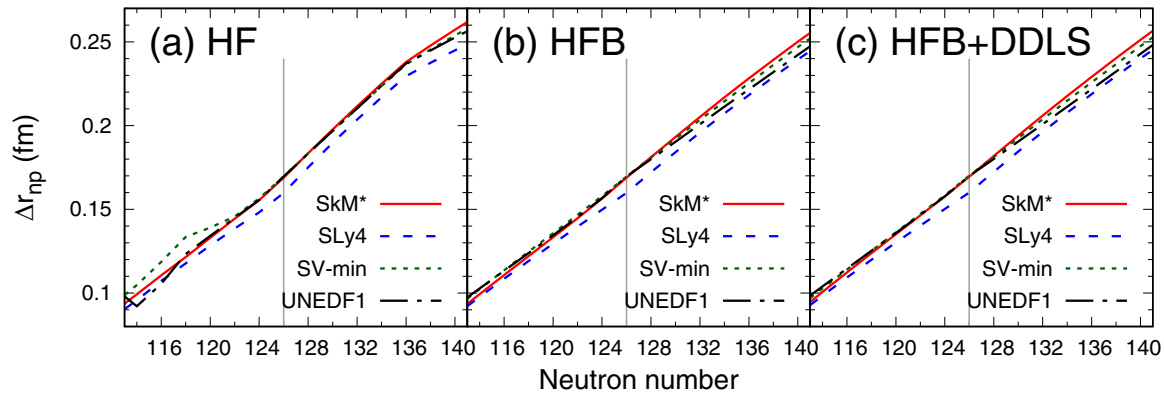

FIG. 5. Neutron skin thickness of Pb isotopes as a function of the neutron number calculated with (a) HF, (b) HFB, and (c) HFB + DDLS.

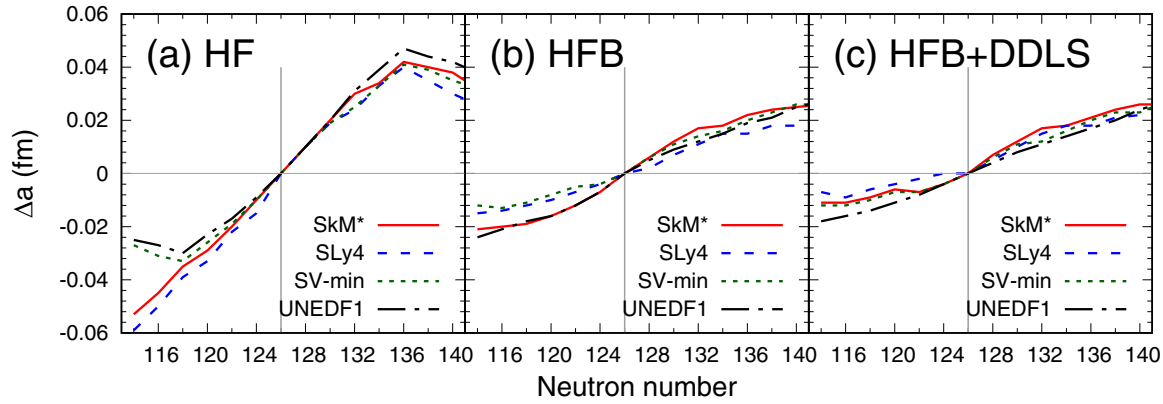

FIG. 6. Absolute difference of the nuclear surface diffuseness measured from ^{208}Pb calculated with (a) HF, (b) HFB, and (c) HFB + DDLS.

useful to study various nuclear structure as exemplified in Refs. [30–32]. To probe the degree of the configuration mixing, we show the diffuseness parameter of the matter density distributions, which can accurately be deduced from proton-elastic scattering [30]. Suppose that the nuclear density is approximated as the two-parameter Fermi distribution (2pF)

$$\rho_{\rm 2pF}(r) = \frac{\rho_c}{1+\exp\left[(r-R)/a\right]}, \tag{16}$$

where ρ_c is determined from the normalization condition $4\pi \int_0^\infty dr\, r^2 \rho_{\rm 2pF}(r) = A$, for given the radius ($R$) and diffuseness ($a$) parameters. As prescribed in Ref. [30], the R and a values are fixed in such a way to minimize the rms deviation of the density distributions obtained by the present calculations. The nuclear diffuseness evolves depending on the characteristics of the sp wave function of the valence neutrons [33]: Nodal (nodeless) orbits near the Fermi level always enhance (reduce) the nuclear surface diffuseness.

Figure 6 displays the absolute difference of the nuclear surface diffuseness of $N > 126$ from that of ^{208}Pb, $\Delta a(N) = a(N) - a(N_0 = 126)$. The Δa becomes largest in the HF case at $N = 136$ and reduces rapidly for $N > 136$. This is simply because the $1g_{9/2}$ orbit plays a role in enhancing the nuclear diffuseness at $126 < N < 136$ and the occupation of the $0i_{11/2}$ orbit reduces the nuclear diffuseness at $N > 136$. With the pairing interaction, the HFB case, the enhancement of the nuclear diffuseness is not significant compared to the HF case due to the occupation of the "sharp" $0i_{11/2}$ and $0j_{15/2}$ orbits in addition to the occupation of the "diffused" $1g_{9/2}$ orbit.

To see changes in the densities near the nuclear surface, Fig. 7 compares the sp densities of the valence neutrons, defined by $\rho_v(r) = 4\pi r^2 \sum_{i\in v} |V_i(r)|^2$, of ^{214}Pb with the SkM* interaction for the HF, HFB, and HFB + DDLS calculations. Obviously, a clear two-peak structure is found for the HF calculation originating in the $(1g_{9/2})^2$ configuration. As we already discussed, a shrinkage of the $1g_{9/2}$ orbit and the mixing of $0i_{11/2}$ and $0j_{15/2}$ orbits occur with the pairing interaction. Since the nodeless high angular momentum orbits, i.e., the $0i_{11/2}$ and $0j_{15/2}$ orbits, are mixed, the nuclear surface diffuseness is reduced [33]. A systematic measurement of the nuclear surface diffuseness will reveal the degree of the configuration mixing of Pb isotopes for $N > 126$, which is closely related to the core swelling phenomenon.

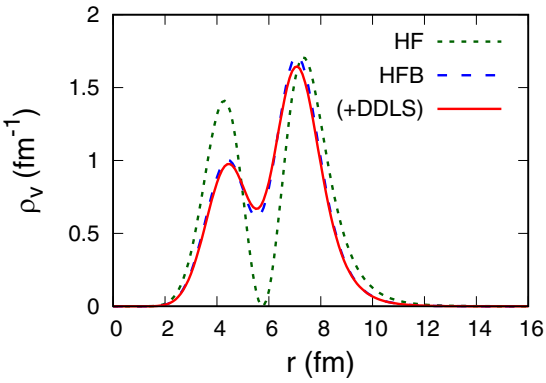

FIG. 7. Valence neutron densities of ^{214}Pb with the SkM* interaction. See text for details.

V. CONCLUSION

We have revisited the kink behavior of the isotope shift of the charge radius of Pb isotopes at $N > 126$ in terms of the Skyrme Hartree-Fock-Bogoliubov (HFB) theory. Four standard Skyrme-density functionals, SkM*, SLy4, SV-min, and UNEDF1 have been employed. The strengths of the pairing interaction for each Skyrme functional were determined so as to reproduce the pairing-rotational energy around ^{208}Pb, and the parameters of the density-dependent spin-orbit (DDLS) term were fixed for the first time for the Skyrme density functionals.

With the present choice of the pairing interaction, the kink behavior of the isotope shift of the charge radius can be reproduced fairly well, while no kink appears without the pairing interaction. The DDLS interaction further increases the charge radius but its effect is small compared to the pairing correlations. In Pb isotopes at $N > 126$, the pairing correlations act to induce the mixing of the $0i_{11/2}$ orbit and the shrinkage of the $1g_{9/2}$ orbits. Since the $0i_{11/2}$ orbit is smaller than the $1g_{9/2}$ orbit, in total the "valence" neutron orbits shrink and "core" swelling occurs as interpreted in Ref. [4]. This novel pairing core swelling effect is imprinted in the isotope shifts of the

charge radius at $N > 126$ as well as the density profile near the nuclear surface exhibiting a moderate change of the nuclear surface diffuseness. It is interesting to explore the possible mechanism of the charge radius kink in different mass regions as it reflects configurations near the Fermi level, which were recently realized in Sn isotopes at $N > 132$ [34].

ACKNOWLEDGMENTS

This work was in part supported by JSPS KAKENHI Grant No. 18K03635. We acknowledge the Collaborative Research Program 2021, Information Initiative Center, Hokkaido University.

[1] I. Angeli and K. P. Marinova, At. Data Nucl. Data Tables **99**, 69 (2013).
[2] R. F. Garcia Ruiz, M. L. Bissell, K. Blaum, A. Ekström, N. Frömmgen, G. Hagen, M. Hammen, K. Hebeler, J. D. Holt, G. R. Jansen *et al.*, Nat. Phys. **12**, 594 (2016).
[3] M. Tanaka, M. Takechi, M. Fukuda, D. Nishimura, T. Suzuki, Y. Tanaka, T. Moriguchi, D. S. Ahn, A. Aimaganbetov, M. Amano *et al.*, Phys. Rev. Lett. **124**, 102501 (2020).
[4] W. Horiuchi and T. Inakura, Phys. Rev. C **101**, 061301(R) (2020).
[5] D. Vautherin and D. M. Brink, Phys. Rev. C **5**, 626 (1972).
[6] P.-G. Reinhard and H. Flocard, Nucl. Phys. A **584**, 467 (1995).
[7] H. Nakada and T. Inakura, Phys. Rev. C **91**, 021302(R) (2015).
[8] S. A. Fayans, S. V. Tolokonnikov, E. L. Trykov, and D. Zawischa, Nucl. Phys. A **676**, 49 (2000).
[9] T. Day Goodacre, A. V. Afanasjev, A. E. Barzakh, B. A. Marsh, S. Sels, P. Ring, H. Nakada, A. N. Andreyev, P. Van Duppen, N. A. Althubiti, B. Andel, D. Atanasov, J. Billowes, K. Blaum, T.E. Cocolios, J.G. Cubiss, G.J. Farooq-Smith, D.V. Fedorov, V.N. Fedosseev, K.T. Flanagan *et al.*, Phys. Rev. Lett. **126**, 032502 (2021).
[10] T. Day Goodacre, A. V. Afanasjev, A. E. Barzakh, L. Nies, B. A. Marsh, S. Sels, U. C. Perera, P. Ring, F. Wienholtz, and A. N. Andreye, Phys. Rev. C **104**, 054322 (2021)
[11] K. Bennaceur and J. Dobaczewski, Comput. Phys. Commun. **168**, 96 (2005).
[12] J. Bartel, P. Quentin, M. Brack, C. Guet, and H. Håkansson, Nucl. Phys. A **386**, 79 (1982).
[13] E. Chabanat, P. Bonche, P. Haensel, J. Mayer, and R. Schaeffer, Nucl. Phys. A **627**, 710 (1997).
[14] P. Klüpfel, P.-G. Reinhard, T. J. Bürvenich, and J. A. Maruhn, Phys. Rev. C **79**, 034310 (2009).
[15] M. Kortelainen, J. McDonnell, W. Nazarewicz, P. G. Reinhard, J. Sarich, N. Schunck, M. V. Stoitsov, and S. M. Wild, Phys. Rev. C **85**, 024304 (2012).
[16] H. Nakada, Phys. Rev. C **92**, 044307 (2015).
[17] H. Kurasawa and T. Suzuki, Prog. Theor. Exp. Phys. **2019**, 113D01 (2019).
[18] W. Satuła, J. Dobaczewski, and W. Nazarewicz, Phys. Rev. Lett. **81**, 3599 (1998).
[19] T. Duguet, P. Bonche, P.-H. Heenen, and J. Meyer, Phys. Rev. C **65**, 014311 (2001).
[20] G. F. Bertsch, C. A. Bertulani, W. Nazarewicz, N. Schunck, and M. V. Stoitsov, Phys. Rev. C **79**, 034306 (2009).
[21] N. Hinohara and W. Nazarewicz, Phys. Rev. Lett. **116**, 152502 (2016).
[22] S. Gales, G. M. Crawley, D. Weber, and B. Zwieglinski, Phys. Rev. C **18**, 2475 (1978).
[23] M. J. Martin, Nucl. Data Sheets **70**, 315 (1993), data extracted from the ENSDF database for $A = 207$, revision of October 25, 2005, NNDC online service.
[24] M. J. Martin, Nucl. Data Sheets **63**, 723 (1991), data extracted from the ENSDF database for $A = 209$, revision of October 25, 2005, NNDC online service.
[25] https://www.nndc.bnl.gov/.
[26] P. Aufmuth, K. Heilig, and A. Steudel, At. Data Nucl. Data Tables **37**, 455 (1987).
[27] S. Goriely, Nucl. Phys. A **933**, 68 (2015).
[28] W. Horiuchi and T. Inakura, Prog. Theor. Exp. Phys. **2021**, 103D02 (2021).
[29] U. C. Perera, A. V. Afanasjev, and P. Ring, Phys. Rev. C **104**, 064313 (2021).
[30] S. Hatakeyama, W. Horiuchi, and A. Kohama, Phys. Rev. C **97**, 054607 (2018).
[31] V. Choudhary, W. Horiuchi, M. Kimura, and R. Chatterjee, Phys. Rev. C **102**, 034619 (2020).
[32] V. Choudhary, W. Horiuchi, M. Kimura, and R. Chatterjee, Phys. Rev. C **104**, 054313 (2021).
[33] W. Horiuchi, Prog. Theor. Exp. Phys. **2021**, 123D01 (2021).
[34] C. Gorges, L. V. Rodríguez, D. L. Balabanski, M. L. Bissell, K. Blaum, B. Cheal, R. F. Garcia Ruiz, G. Georgiev, W. Gins, H. Heylen, A. Kanellakopoulos, S. Kaufmann, M. Kowalska, V. Lagaki, S. Lechner, B. Maass, S. Malbrunot-Ettenauer, W. Nazarewicz, R. Neugart, G. Neyens *et al.*, Phys. Rev. Lett. **122**, 192502 (2019).